LETTERS
PUBLISHED ONLINE: 18 SEPTEMBER 2011 | DOI: 10.1038/NMAT3120
nature materials

Kinetic frustration and the nature of the magnetic and paramagnetic states in iron pnictides and iron chalcogenides

Z. P. Yin[1,2]*, K. Haule[1] and G. Kotliar[1]

The iron pnictide and chalcogenide compounds are a subject of intensive investigations owing to their surprisingly high temperature superconductivity[1]. They all share the same basic building blocks, but there is significant variation in their physical properties, such as magnetic ordered moments, effective masses, superconducting gaps and transition temperature (T_c). Many theoretical techniques have been applied to individual compounds but no consistent description of the microscopic origin of these variations is available[2]. Here we carry out a comparative theoretical study of a large number of iron-based compounds in both their magnetic and paramagnetic states. Taking into account correlation effects and realistic band structures, we describe well the trends in all of the physical properties such as the ordered moments, effective masses and Fermi surfaces across all families of iron compounds, and find them to be in good agreement with experiments. We trace variation in physical properties to variations in the key structural parameters, rather than changes in the screening of the Coulomb interactions. Our results also provide a natural explanation of the strongly Fermi-surface-dependent superconducting gaps observed in experiments[3].

The iron pnictides/chalcogenides are Hund's metals. In these systems the Coulomb interaction among the electrons is not strong enough to fully localize them, but it significantly slows them down, such that low-energy emerging quasiparticles have a substantially enhanced mass[4]. This enhanced mass emerges not because of the Hubbard interaction U, but because of the Hund's rule interactions that tend to align electrons with the same spin but different orbital quantum numbers when they find themselves on the same iron atom[4].

A central puzzle in this field is posed by the variation of the ordered magnetic moment across the iron pnictides/chalcogenides series. In the fully localized picture, the atom resides in a single valence; therefore, the ordered moment is equal to the atomic moment (4 μ_B per iron), possibly reduced by quantum fluctuations. This picture is realized in cuprate superconductors where quantum fluctuations reduce the Cu^{2+} moment by 20%. In the fully itinerant weak-coupling picture, such as the spin-density wave (SDW) in chromium metal, the ordered moment is related to the degree of Fermi-surface nesting. It is now clear that the iron pnictides are not well described by either the fully localized or fully itinerant picture, nor by the density functional theory (DFT), which greatly overestimates the ordered magnetic moments (see Supplementary Information). It has been advocated that the shortcomings of DFT can be circumvented by incorporating the physics of long-wavelength fluctuations[5]. Here we take the opposite perspective. Although critical long-wavelength fluctuations certainly play a role near the phase-transition lines, we will show that the local fluctuations on the iron atom can account for the correct trend of magnetic moments and correlation strength in iron pnictide/chalcogenide layered compounds.

Using the combination of DFT and dynamical mean field theory (DFT + DMFT) (see Supplementary Information for details), we studied two different real-space orderings, the SDW ordering, characterized by wave vector $(\pi, 0, \pi)$ (this vector is written in coordinates with one iron atom per unit cell), which is experimentally found in iron arsenide compounds, and $(\pi/2, \pi/2, \pi)$ ordering, denoted by the double-stripe SDW (DSDW). The latter was found experimentally in FeTe. Figure 1a shows our theoretical results for the ordered moment in both phases together with experimentally determined values[6–13] from across all known families of iron-based superconducting compounds. There is an overall good agreement between theory and experiment; in particular, LaFePO is predicted to be non-magnetic, most 1111 and 122 compounds have an ordered moment below 1.0 μ_B (ref. 14) and FeTe orders with a DSDW moment of 2.1 μ_B.

We now explain the variation of the ordered moment in terms of real-space and momentum-space concepts. The size of the fluctuating local moment, which can be extracted from neutron scattering experiments, gives an upper bound to the size of the ordered magnetic moment and is also plotted in Fig. 1a. It was computed from the atomic histogram in Fig. 2c, which shows the percentage of time the iron 3d electrons spend in various atomic configurations when the system is still in its paramagnetic state. Only high-spin states, which carry a large weight as a result of the Hund's rule coupling in iron, are shown (see also Supplementary Information for the complete histogram).

In a correlated Fermi liquid, the spin excitations are described in terms of individual particle–hole pair excitations and their collective motion. Their residual interaction can lead to a magnetic state when the particle–hole excitations condense at non-zero wave vector. A large quasiparticle mass naturally facilitates this condensation; hence, we expect that the size of the ordered moment will correlate with the mass of the quasiparticles. In Fig. 1b we show separately the quasiparticle mass for all iron 3d orbitals in the paramagnetic state and we normalize it to its band value. Clearly there is some correlation between mass enhancement in Fig. 1b and ordered magnetic moment in Fig. 1a across various families of iron-based compounds. In particular, correlations are too weak for ordering in LaFePO, whereas very heavy quasiparticles in FeTe produce a large moment of 2.1 μ_B. However, there are other factors presented below, such as kinetic frustration, orbital differentiation

[1]Department of Physics and Astronomy, Rutgers University, Piscataway, New Jersey 08854, USA, [2]Department of Physics and Astronomy, Stony Brook University, Stony Brook, New York 11794, USA. *e-mail: yinzping@physics.rutgers.edu.

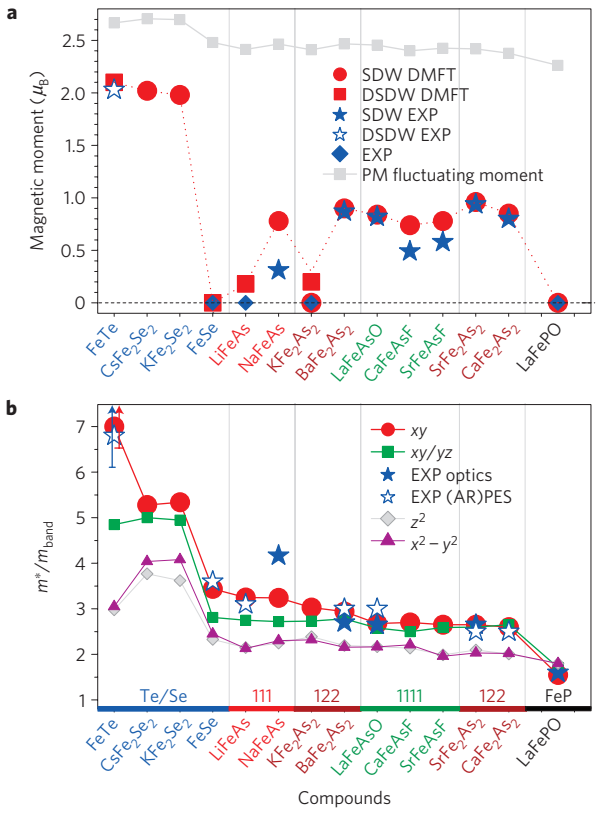

Figure 1 | Ordered magnetic moments and mass enhancements in iron-based compounds. a, The DFT + DMFT calculated and experimental[6–13] iron magnetic moments in the SDW and DSDW states. Also shown is the calculated fluctuating moment in the paramagnetic (PM) state. **b**, The DFT + DMFT-calculated mass enhancement m^*/m_{band} of the iron 3*d* orbitals in the paramagnetic state and the low-energy effective mass enhancement obtained from optical spectroscopy experiments[16–19] and (angle-resolved) photoemission spectroscopy experiments[20–24].

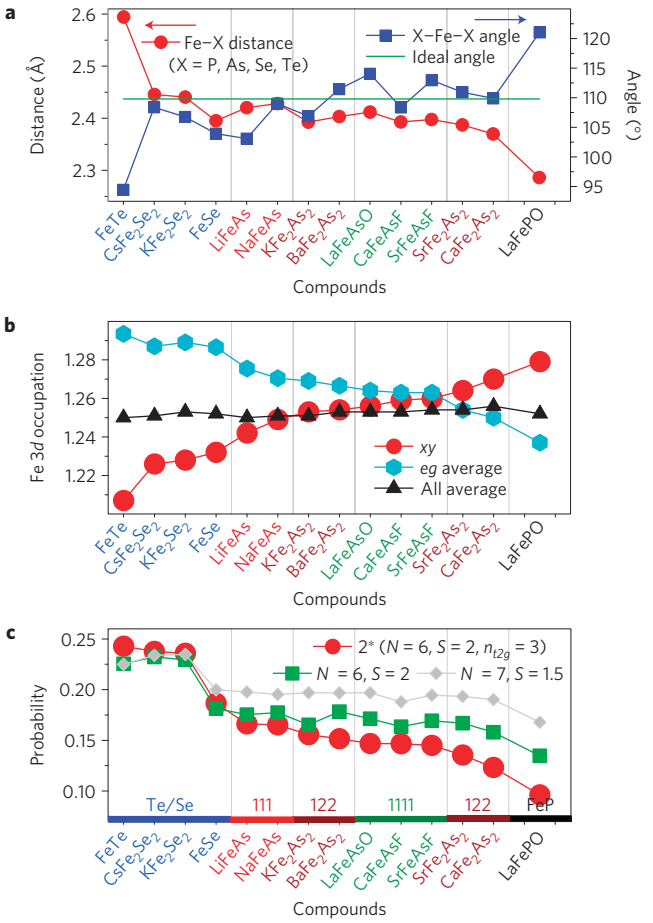

Figure 2 | Structure, orbital occupation and probability of selected atomic states of iron. a, The Fe-X (X = P, As, Se and Te) distance and X-Fe-X angle in iron-based compounds, where the two X atoms are in the same *ab* plane. Note this angle is different from the X-Fe-X angle where the two X atoms are in different *ab* planes. **b**, The orbital occupation of the *xy* orbital and the average values for the *eg* orbitals and all five orbitals. **c**, The probability of selected atomic configurations of iron where $N(S)$ is the total number (spin) of iron 3*d* electrons in the atomic configuration.

and Fermi-surface shape, which together conspire to produce the magnetic orderings shown in Fig. 1a.

The quasiparticle mass shown in Fig. 1b is quite moderate in the phosphorus 1111 compound on the right-hand side of Fig. 1b, but correlations are significantly enhanced in arsenic 122 and 1111 compounds. Note, however, that enhancement is not equal in all orbitals, but it is significantly stronger in the $t2g$ orbitals, that is, xz, yz, and xy. The correlations get even stronger in 111 compounds, such as LiFeAs and NaFeAs, and finally jump to significantly larger values of the order of five in selenides KFe_2Se_2 and $CsFe_2Se_2$. Finally, the mass enhancement of the xy orbital in FeTe exceeds a factor of seven when compared with the band mass, which is typical for heavy-fermion materials, but is rarely found in transition-metal compounds. We showed only a lower bound for this mass as the end point of an arrow in Fig. 1b, because the quasiparticles are not yet well formed at the studied temperature $T = 116$ K. Note the strong orbital differentiation in FeTe, with an xz/yz mass of five and an *eg* mass enhancement of only three. This orbital differentiation signals that the material is in the vicinity of an orbital-selective Mott transition, as proposed previously for other iron pnictides[15], where the xy orbital is effectively insulating while other orbitals remain metallic. In Fig. 1b we also show the mass enhancement extracted from optics[16–19] and angle-resolved photoemission spectroscopy (ARPES) (refs 20–24) measurements, and find a good agreement between our theory and experiment when available. The effective mass extracted from ARPES and optics should be compared with that of the $t2g$ orbitals, which contribute most of the spectral weight at low energy.

The large mass enhancement in Hund's metals is due to an orbital blocking mechanism. If the Hund's coupling is very large, only the high-spin states have a finite probability in the atomic histogram. The atomic high-spin ground state has a maximum possible spin $S = 2$, and is orbitally a singlet, which does not allow mixing of the orbitals and leads to orbital blocking, that is, $\langle gs|d_\alpha^\dagger d_\beta|gs\rangle = 0$ when $\alpha \neq \beta$, where $|gs\rangle$ is the atomic ground state in the $3d^6$ configuration and α is the iron orbital index. In the localized limit and in the absence of crystal-field effects, it is possible to derive a low-energy effective Kondo model, which has Kondo coupling for a factor of $(2S+1)^2$ smaller than a model without Hund's coupling[25]. As the Kondo temperature T_K depends on the Kondo coupling I_0 exponentially ($T_K \propto \exp(-1/I_0)$), this results in an enormous mass enhancement of the order of $\exp(((2S+1)^2-1)/I_0)$ when compared with the system with negligible Hund's coupling (see also Supplementary Information).

Having established why heavy quasiparticles form in iron pnictides and chalcogenides, we can now study how the key parameters of the crystal structure control the strength of correlations and other physical properties, keeping the same on-site Coulomb interaction matrix. The Fe–pnictogen distance, shown in

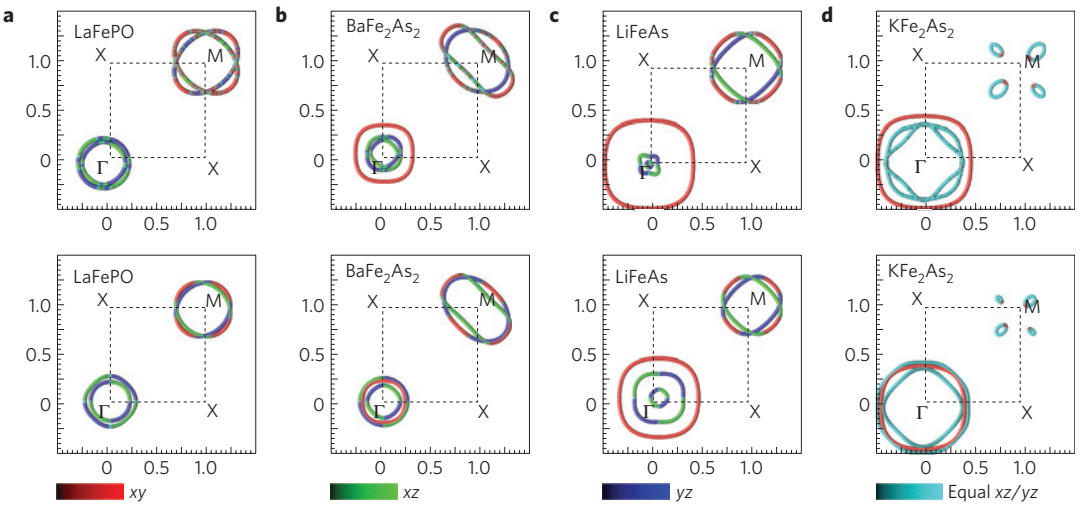

Figure 3 | Fermi surface. a–d, The DFT + DMFT- (top row) and DFT- (bottom row) calculated two-dimensional Fermi surface in the Γ plane ($k_z = 0$) for LaFePO (**a**), $BaFe_2As_2$ (**b**), LiFeAs (**c**) and KFe_2As_2 (**d**). The Fermi surface is coloured in red, green and blue according to its dominating orbital character of *xy*, *xz* and *yz*, respectively. When there is an equal amount of dominating *xz* and *yz* character it is coloured in cyan. Darker colour corresponds to a lower amount of the specific character.

Fig. 2a, controls the overlap between the iron and pnictogen atom and hence makes iron electrons more localized (itinerant) with increasing (decreasing) distance. The largest distance is achieved in compounds with a larger chalcogenide ion, such as in FeTe, which results in very heavy quasiparticles, as seen in Fig. 1b. The variation in distance alters the overall bandwidth moderately. The Hund's orbital blocking mechanism amplifies this variation.

The second key structural parameter is the tetrahedron shape, which is parameterized in terms of the pnictogen–Fe–pnictogen angle, shown in Fig. 2a. This angle is equal to 109.5° for an ideal tetrahedron, and is much smaller in FeTe, where the Te ion is pushed farther away from the iron plane. The shape of the tetrahedron controls the crystal-field levels, which in turn control the orbital occupancies. We show them in Fig. 2b. The average occupation of the iron atom is around $n_d = 6.25$ across all of the compounds studied, which leads to an average orbital occupation of $n_\alpha = 1.25$. A deviation from the ideal angle enhances the crystal-field splittings between *xy* and the degenerate *xz*/*yz* orbital and also changes the splitting between $t2g$ and eg orbitals. Heavier quasiparticles with a smaller quasiparticle bandwidth are more susceptible to the crystal-field splitting; hence, the orbital differentiation is largest in FeTe but very small in LaFePO. The net result of crystal-field splittings and quasiparticle mass is the charge transfer from the $t2g$ to eg orbitals as seen in Fig. 2b, and among $t2g$ orbitals the *xy* orbital loses most charge with increased correlation strength, pushing its occupancy closer to integer filling.

Furthermore, the effective hopping between neighbouring iron atoms has two contributions, one is due to direct Fe–Fe overlap, and the second is indirect hopping through the pnictogen atom. The two contributions to the diagonal hopping $t_{\alpha,\alpha}$ have opposite signs and destructively interfere. For the *xz* and *yz* orbital, the indirect hopping through the pnictogen is larger than the direct Fe–Fe hop. For the *xy* orbital, the two contributions are very similar, and when the pnictogen height is sufficiently large, such as in FeTe, the indirect hop is reduced and the two contributions almost exactly cancel each other, resulting in vanishing effective nearest-neighbour Fe–Fe $t_{xy,xy}$ hopping. This kinetic frustration mechanism contributes to the marked enhancement of the *xy* mass in the FeTe compound.

In itinerant systems, the shape of the Fermi surface, or the Fermi-surface nesting, is relevant for deciding which magnetic ordering wave vector is realized when the residual interactions among the quasiparticles are sufficiently strong. Additional terms, arising from the incoherent part of the electron, become increasingly important as the localization threshold is approached.

In Fig. 3 we show the DFT + DMFT Fermi surface together with DFT predictions. In the moderately correlated end, such as in the phosphorus 1111 compounds, our theoretical predictions match DFT results. However, when correlations become sizable, such as in LaFeAsO or $BaFe_2As_2$, the *xy* orbital starts to play a special role, which results in a slightly modified Fermi-surface shape and character when compared with DFT, while respecting the Luttinger theorem. In $BaFe_2As_2$, DFT predicts that the outer pocket at Γ is of *xz*/*yz* character, whereas DFT + DMFT predicts that the outer pocket is of *xy* character, in agreement with experiments[26]. This effect of growing *xy* pocket at Γ and consequently shrinking of *xz*/*yz* pocket is also apparent in LiFeAs, bringing the DFT + DMFT Fermi surface in better agreement with the experiment of ref. 22.

These changes in the shape of the Fermi surfaces are the momentum-space counterpart of the real-space picture of charge transfer among the iron $3d$ orbitals shown in Fig. 2b. This is because the decrease (increase) of the *xy* (*xz*, *yz*) orbital occupancy results in the increase (decrease) of the hole pocket size. Finally, the Fermi surface of KFe_2As_2 shown in Fig. 3 has only hole pockets around Γ but almost no electron pockets at M; hence, there is no Fermi-surface nesting to facilitate the long-range magnetic order. Indeed, KFe_2As_2 cannot sustain SDW ordering and only a tiny DSDW moment can be stabilized, as shown in Fig. 1a. Although the mass enhancement in KFe_2As_2 and 111 compounds is substantial, the Fermi-surface nesting still plays an important role in stabilizing magnetic ordering.

The fluctuating moment presented in Fig. 1a monotonically increases with increased correlation strength, and constitutes an upper bound to the size of the ordered magnetic moment. However, even when the Fermi-surface nesting is quite good, such as in 1111 and many 122 compounds, the ordered moment is substantially reduced from this upper bound. In the DFT + DMFT theoretical method, the orbital differentiation is responsible for the large overall reduction of the static moment. In very itinerant systems, such as LaFePO, the quasiparticles are too weakly interacting to condense; hence, moderate correlations with a mass enhancement of 1.5 do not sufficiently localize electrons to allow magnetic ordering. In most other compounds, the localization and hence the effective mass increase is substantial only in $t2g$ orbitals,

while *eg* orbitals remain only moderately correlated. Consequently, the ordered magnetic moment is small in *eg* orbitals, which causes only a fraction of the fluctuating moment to order. Only when correlations are very strong and equal in all orbitals, almost the entire fluctuating moment orders. Such an example is provided by $K_{0.8}Fe_{1.6}Se_2$, which is obtained by introducing iron vacancies into KFe_2Se_2, where the entire fluctuating moment of 3.3 μ_B orders (Z. P. Yin, K. Haule, & G. Kotliar, manuscript in preparation (2011)).

We conclude with some experimental consequences of the theory. We placed FeTe at the verge of an orbitally selective Mott transition. This idea can be tested by applying uniaxial pressure on the FeTe. Compressive strain along the *c* axis should restore coherence in the transport properties. Our results also support a natural origin for a particle–hole asymmetry in doping the parent compounds. Reducing the iron occupancy of the 3*d* orbital brings the occupancy of the *xy* orbital closer to unity, and increases the correlation strength, which in turn strengthens the magnetic moment. This has been observed in ARPES studies of the $BaFe_2As_2$ family[27].

The intermediate correlation strength and large degeneracy is a fertile ground for superconductivity, whereas large orbital differentiation is harmful. Hence, we expect the highest critical temperature to be found around the region of intermediate m^* in Fig. 1b and equal orbital occupancy in Fig. 2b. The optimal correlation strength criterion also operates on the level of individual orbitals. We predict that the larger mass enhancement and the consequent incoherence of the *xy* orbital leads to a smaller superconducting gap on the most outside hole pocket centred at Γ, which is mostly of *xy* character.

Methods

We use fixed Coulomb interaction parameters for all materials in our DFT+DMFT calculations to keep a parameter-free spirit and to demonstrate that the variations in the calculated physical properties are mainly due to the variations in the key structural parameters, rather than changes in the screening of the Coulomb interactions. The detail of the method is included in Supplementary Information.

Received 21 April 2011; accepted 16 August 2011; published online 18 September 2011; corrected online 23 September 2011

References

1. Kamihara, Y. *et al.* Iron-based layered superconductor $La[O_{1-x}F_x]FeAs$ ($x = 0.05$–0.12) with $T_c = 26$ K. *J. Am. Chem. Soc.* **130,** 3296–3297 (2008).
2. Paglione, J. & Greene, R. L. High-temperature superconductivity in iron-based materials. *Nature Phys.* **6,** 645–658 (2010).
3. Ding, H. *et al.* Observation of Fermi-surface-dependent nodeless superconducting gaps in $Ba_{0.6}K_{0.4}Fe_2As_2$. *Europhys. Lett.* **83,** 47001 (2008).
4. Haule, K. & Kotliar, G. Coherence-incoherence crossover in the normal state of iron-oxypnictides and importance of the Hund's rule coupling. *New J. Phys.* **11,** 025021 (2009).
5. Mazin, I. I & Johannes, M. D. A key role for unusual spin dynamics in ferropnictides. *Nature Phys.* **5,** 141–145 (2009).
6. Bao, W. *et al.* Incommensurate magnetic order in the α-Fe(Te,Se) superconductor systems. *Phys. Rev. Lett.* **102,** 247001 (2009).
7. Yu, W. Q. *et al.* ^{23}Na and ^{75}As NMR study of antiferromagnetism and spin fluctuations on NaFeAs single crystals. *Phys. Rev. B* **83,** 132501 (2011).
8. Huang, Q. *et al.* Magnetic order in $BaFe_2As_2$, the parent compound of the FeAs based superconductors in a new structural family. *Phys. Rev. Lett.* **101,** 257003 (2008).
9. Li, H-F. *et al.* Phase transitions and iron-ordered moment form factor in LaFeAsO. *Phys. Rev. B* **82,** 064409 (2010).
10. Xiao, Y. *et al.* Magnetic order in $CaFe_{1-x}Co_xAsF$ ($x = 0$, 0.06, 0.12) superconductor compounds. *Phys. Rev. B* **79,** 060504 (2009).
11. Xiao, Y. *et al.* Neutron diffraction study on phase transition and thermal expansion of SrFeAsF. *Phys. Rev. B* **81,** 094523 (2010).
12. Zhao, J. *et al.* Spin and lattice structure of single crystal $SrFe_2As_2$. *Phys. Rev. B* **78,** 140504 (2008).
13. Goldman, A. I. *et al.* Lattice and magnetic instabilities in $CaFe_2As_2$: A single crystal neutron diffraction study. *Phys. Rev. B* **78,** 100506 (2008).
14. Yin, Z. P., Haule, K. & Kotliar, G. Magnetism and charge dynamics in iron pnictides. *Nature Phys.* **7,** 294–297 (2011).
15. de' Medici, L. *et al.* Orbital-selective Mott transition out of band degeneracy lifting. *Phys. Rev. Lett.* **102,** 126401 (2009).
16. Hu, W. Z. *et al.* Optical study on the spin-density wave properties in single crystalline $Na_{1-\delta}FeAs$. *Phys. Rev. B* **80,** 100507 (2009).
17. Hu, W. Z. *et al.* Origin of the spin density wave instability in AFe_2As_2 (A = Ba, Sr) as revealed by optical spectroscopy. *Phys. Rev. Lett.* **101,** 257005 (2008).
18. Chen, Z. G. *et al.* Optical spectroscopy study on single crystalline LaFeAsO. *Phys. Rev. B* **81,** 100502 (2010).
19. Qazilbash, M. M. *et al.* Electronic correlations in the iron pnictides. *Nature Phys.* **5,** 647–650 (2009).
20. Tamai, A. *et al.* Strong electron correlations in the normal state of $FeSe_{0.42}Te_{0.58}$. *Phys. Rev. Lett.* **104,** 097002 (2010).
21. Yamasaki, A. *et al.* Electron correlation in FeSe superconductor studied by bulk-sensitive photoemission spectroscopy. *Phys. Rev. B* **82,** 184511 (2010).
22. Borisenko, S. V. *et al.* Superconductivity without magnetism in LiFeAs. *Phys. Rev. Lett.* **105,** 067002 (2010).
23. Yi, M. *et al.* Unconventional electronic reconstruction in undoped $(Ba,Sr)Fe_2As_2$ across the spin density wave transition. *Phys. Rev. B* **80,** 174510 (2009).
24. Wang, Q. *et al.* Uniaxial 'nematic-like' electronic structure and Fermi surface of untwinned $CaFe_2As_2$. Preprint at http://arxiv.org/abs/1009.0271 (2010).
25. Okada, I. & Yosida, K. Singlet ground state of the localized *d*-electrons coupled with conduction electrons in metals. *Prog. Theor. Phys.* **49,** 1483–1502 (1973).
26. Zhang, Y. *et al.* Orbital characters of bands in iron-based superconductor $BaFe_{1.85}Co_{0.15}As_2$. *Phys. Rev. B* **83,** 054510 (2011).
27. Yi, M. *et al.* Electronic structure of the $BaFe_2As_2$ family of iron-pnictide superconductors. *Phys. Rev. B* **80,** 024515 (2009).

Acknowledgements

Z.P.Y. and G.K. were supported by NSF DMR-0906943; K.H. was supported by NSF DMR-0746395. Part of the work (Z.P.Y.) was carried out under the auspices of a DoD National Security Science and Engineering Faculty Fellowship, through AFOSR grant FA 9550-10-1-0191. Acknowledgement (K.H.) is made to the donors of the American Chemical Society Petroleum Research Fund for partial support of this research.

Author contributions

Z.P.Y. carried out the calculations. K.H. developed the DMFT code. Z.P.Y., K.H. and G.K. analysed the results and wrote the paper. Z.P.Y. led the project.

Additional information

The authors declare no competing financial interests. Supplementary information accompanies this paper on www.nature.com/naturematerials. Reprints and permissions information is available online at http://www.nature.com/reprints. Correspondence and requests for materials should be addressed to Z.P.Y.

ERRATUM

Kinetic frustration and the nature of the magnetic and paramagnetic states in iron pnictides and iron chalcogenides

Z. P. Yin, K. Haule and G. Kotliar

Nature Materials http://dx.doi.org/10.1038/nmat3120 (2011); published online 18 September 2011; corrected online 23 September 2011.

In the version of this Letter originally published, $BaFe_2Se_2$ should have been $BaFe_2As_2$ in Figs 1 and 2. This error has been corrected in all versions of the Letter.